

Article

Catalytic Performances of Sn-Beta Catalysts Prepared from Different Heteroatom-Containing Beta Zeolites for the Retro-Aldol Fragmentation of Glucose

Ricardo Navar¹, Luca Botti², Giulia Tarantino²  and Ceri Hammond^{2,*}¹ Cardiff Catalysis Institute, Cardiff University, Park Place, Cardiff CF10 3AT, UK; navarr@cardiff.ac.uk² Department of Chemical Engineering, Imperial College London, London SW7 2AZ, UK;

l.botti20@imperial.ac.uk (L.B.); g.tarantino@imperial.ac.uk (G.T.)

* Correspondence: ceri.hammond@imperial.ac.uk

Abstract: Beta zeolites with different heteroatoms incorporated into the lattice at two loadings (Si/M = 100 or 200, where M = Al, Fe, Ga, B) were hydrothermally synthesised and used as starting materials for the preparation of Sn-Beta using Solid-State Incorporation. ¹¹⁹Sn CPMG MAS NMR showed that various Sn species were formed, the distribution of which depended on the identity of the initial heteroatom and the original Si/M ratio. The final Sn-Beta materials (with Si/Sn = 200) were explored as catalysts for the retro-aldol fragmentation of glucose to α -hydroxy-esters in the continuous regime. Amongst these materials, B-derived Sn-Beta was found to exhibit improved levels of selectivity and stability, particularly compared to Sn-Beta catalysts synthesised from commercially available Al-Beta materials, achieving a combined yield of methyl lactate and methyl vinyl glycolate > 80% at short times on the stream. Given that B atoms can be removed from the Beta lattice in mild conditions without the use of highly concentrated acidic media, this discovery demonstrates that B-Beta is an attractive starting material for the future post-synthetic preparation of Lewis acidic zeolites.

Keywords: zeolites; Lewis acid; biomass; retro-aldol fragmentation; catalysis

**Citation:** Navar, R.; Botti, L.;

Tarantino, G.; Hammond, C.

Catalytic Performances of Sn-Beta Catalysts Prepared from Different Heteroatom-Containing Beta Zeolites for the Retro-Aldol Fragmentation of Glucose. *Reactions* **2022**, *3*, 265–282. <https://doi.org/10.3390/reactions3020020>

Academic Editor: Dmitry Yu. Murzin

Received: 14 March 2022

Accepted: 2 May 2022

Published: 12 May 2022

Publisher's Note: MDPI stays neutral with regard to jurisdictional claims in published maps and institutional affiliations.



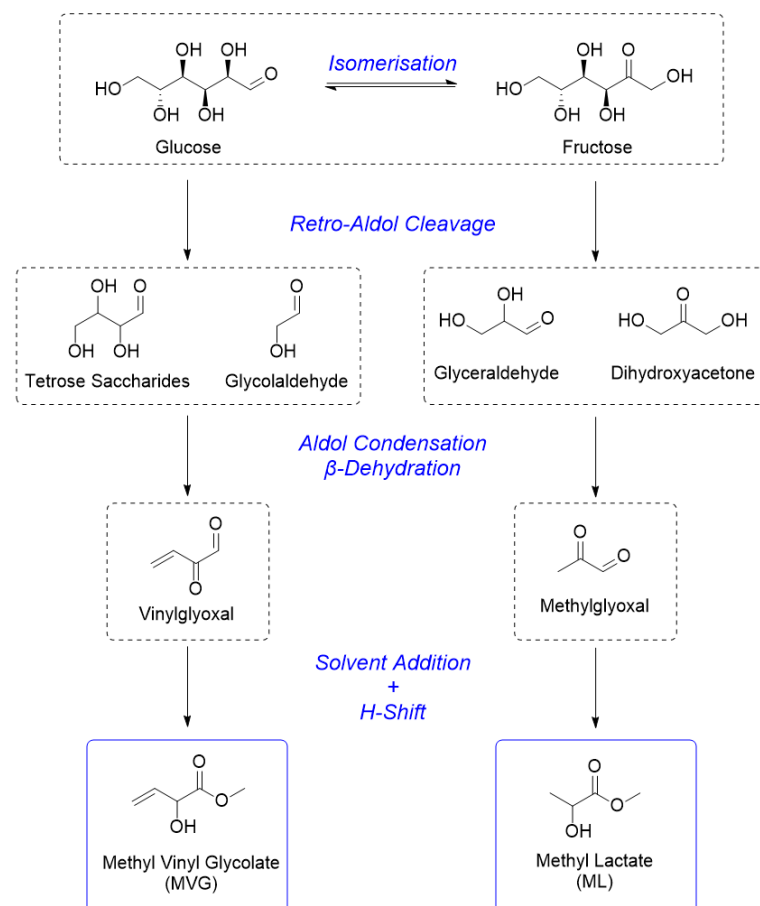
Copyright: © 2022 by the authors. Licensee MDPI, Basel, Switzerland. This article is an open access article distributed under the terms and conditions of the Creative Commons Attribution (CC BY) license (<https://creativecommons.org/licenses/by/4.0/>).

1. Introduction

Lewis acidic zeolites have emerged as state-of-the-art catalysts for the conversion of biomass to commodity chemicals over the past decade, due to their high levels of activity and selectivity. Zeolites are crystalline microporous materials which can exhibit a wide array of catalytic properties depending on their precise composition (i.e., the choice of metal and metal loading) and topology [1–4]. In the context of biomass conversion, the most notable Lewis acidic zeolite is the stannosilicate catalyst Sn-Beta. Sn-Beta is a siliceous zeolite within which small amounts of Lewis acidic Sn(IV) atoms are isomorphously substituted into the three-dimensional lattice. The presence of isolated Sn(IV) atoms has been shown to endow the material with levels of Lewis acidity suitable for the conversion of biomass into various bio-based compounds of industrial interest [5–7]. Methyl lactate (ML) [8] and methyl vinyl glycolate (MVG) [9], for instance, are the main α -hydroxy-esters that can be produced following the cleavage of glucose in the presence of Sn-Beta (Scheme 1). These compounds are highly sought after due to their potential as monomers for the synthesis of bioplastics, or as precursors for surfactant production.

The synthesis of Lewis acidic zeolites such as Sn-Beta can be achieved by two generalised approaches. The first involves conventional hydrothermal synthesis (bottom-up), during which an appropriate metal precursor, such as SnCl₄, is added to the synthesis gel, resulting in the direct incorporation of the metal into the lattice during crystallisation at an elevated temperature and pressure. Alternatively, Sn-Beta can be synthesised by the post-synthetic treatment of an existing zeolite (top-down). In such cases, a previously prepared

zeolite is treated to create vacant lattice sites [10,11], into which Sn can be incorporated in a subsequent synthetic step [12]. The advantages of such a top-down approach (also known as ‘demetallation–remetallation’) [13] include the avoidance of the long crystallisation times associated with hydrothermal Sn-Beta synthesis, and high degrees of synthetic flexibility in terms of choice of the metal and the final metal loading [14–17]. Amongst the top-down methods, Solid-State Incorporation (SSI) is an attractive method in which the desired heteroatom is introduced into the vacant tetrahedral framework sites by a combination of mechanochemistry and thermal treatment, thereby avoiding the generation of aqueous metal streams [18,19].



Scheme 1. Sn-Beta catalysed conversion of glucose to ML and MVG.

A common step in all demetallation–remetallation strategies is the preparation of a zeolite containing vacant lattice sites, suitable for the eventual hosting of the desired Sn heteroatom. This is typically achieved by pre-treating a parent zeolite material at an elevated temperature in concentrated acidic media, resulting in the removal of an original heteroatom [13,18,20–22]. In previous demetallation–remetallation studies, aluminosilicates have almost exclusively been employed as the parent zeolite, primarily due to their commercial availability and the ease of incorporating Al into the lattice of several zeolite structures. However, a variety of other metal-containing zeolites could also act as parent materials for the preparation of post-synthetic Sn-Beta. These include zeolites containing B, Fe and Ga, amongst others, which are also known to be prone to demetallation in appropriate conditions. Notably, such zeolites exhibit a large discrepancy between their ease of demetallation. In particular, B-derived zeolites have been shown to be particularly amenable to demetallation in very mild conditions, because boron is primarily trigonally coordinated, and is thus susceptible to nucleophilic attack by water [23–25]. Furthermore, the use of different heteroatom-containing zeolite materials as precursors for Sn-Beta syn-

thesis could also provide access to final catalysts exhibiting different levels of performance. However, to the best of our knowledge, no study has yet investigated the catalytic properties of otherwise-analogous Sn-Beta samples prepared from hydrothermally synthesised zeolite parents containing different original heteroatoms.

As such, this study investigates the kinetic properties of a variety of Sn-Beta samples prepared by SSI, each prepared from different hydrothermally synthesised Al-, B-, Fe-, and Ga-Beta parent materials. The aim is to determine the impact of the use of different heteroatom-containing zeolites as parent materials for the top-down Sn-Beta synthesis. The characterisation of the synthesised catalysts is performed by means of X-ray Diffraction (XRD), porosimetry, Diffuse Reflectance Infrared Fourier Transform Spectroscopy (DRIFTS), Scanning Electron Microscopy (SEM), Inductively Coupled Plasma Mass Spectroscopy (ICP-MS), and ^{119}Sn Magic Angle Spinning Nuclear Magnetic Resonance using the Carr-Purcell-Meiboom-Gill echo train acquisition method (^{119}Sn CPMG MAS NMR). The kinetic performances of the resulting catalysts are evaluated for the continuous conversion of glucose to α -hydroxy ester compounds (ML and MVG), allowing the activity, selectivity, and stability of the series of catalysts to be determined in a rigorous manner.

2. Materials and Methods

2.1. Materials

Tetraethylammonium hydroxide (TEAOH, 35 wt.% in water), aluminium chloride (AlCl_3 , $\geq 99.99\%$), ferric chloride (FeCl_3 , $\geq 97\%$), gallium chloride (GaCl_3 , $\geq 99.99\%$), boric acid (H_3BO_3 , $\geq 99.5\%$), tetraethylorthosilicate (TEOS, $\geq 99\%$), potassium chloride ($\geq 99\%$), and hydrofluoric acid (48 wt.% in water, $\geq 99.99\%$) were used for the synthesis of the Beta zeolites. All of the reactants were obtained from Merck Life Science UK Limited (Dorset, UK), and were used without any further treatment. Commercial Al-Beta (NH_4^+ -form, Si/M = 19) was purchased from ZeolystTM.

2.2. Catalyst Synthesis

The M-Beta zeolites were synthesised using fluoride ions as a mineraliser, adapting the procedure described in Ref. [14]. In a typical synthesis, 30.6 g TEOS was added to 33.4 g TEAOH under constant stirring at 450 rpm. After 60–90 min, one phase was observed and 0.734 mmol of the metal precursor (FeCl_3 , AlCl_3 , GaCl_3 , and H_3BO_3) corresponding to an Si:M molar ratio of 200:1 was added and left stirring at 450 rpm until the adequate water ratio was reached, typically at 16 h. Afterwards, 3.3 g of HF was added to form a solid gel. The final molar ratios of the gels were 0.0050M:1.0SiO₂:0.54TEAOH:0.54HF:8.5H₂O, where M corresponds to the indicated metal. The gels were transferred into a stainless-steel autoclave with PTFE liners and placed into an oven held at a temperature of 140 °C for 7 days. The zeolites were then filtered and washed with water (2.0 L g⁻¹), and subsequently dried at 110 °C overnight. The removal of the residual Structure Directing Agent (SDA) was achieved by heating the synthesised material to 550 °C for 6 h at 2 °C min⁻¹ in static air. The samples were denoted 'M-Beta', with M corresponding to the metal being incorporated.

Al-Beta and B-Beta with Si:M molar ratios of 100 were prepared following the general procedure described above, albeit with the addition of 1.47 mmol AlCl_3 and H_3BO_3 , respectively.

2.3. Post-Synthetic Modification of M-Beta Zeolites by Solid-State Incorporation

The post-synthetic SSI was conducted as described in Ref. [26]. For simplicity, and to provide a fair comparison for all of the materials, all of the parental Beta zeolites were demetallated in 13 M HNO_3 (20 mL g⁻¹ of zeolite) at 100 °C for 20 h. The demetallated samples were filtered, washed with water, and dried at 110 °C overnight. Subsequently, the incorporation of Sn was undertaken in order to fill the vacant lattice sites of the demetallated zeolites. This was achieved by grinding the demetallated materials with the required quantity of tin (II) acetate for 10 min. Thereafter, the solid mixtures were heated in a combustion furnace (Carbolite MTF12/38/400, Carbolite Gero, Sheffield, UK) to 550 °C

(10 °C min⁻¹ ramp rate) in a nitrogen flow (60 mL min⁻¹). The catalysts were held at 550 °C for three hours before the gas flow was changed to air (60 mL min⁻¹), and this was maintained at the same temperature for an additional 3 h.

2.4. Catalyst Characterisation

X-ray diffraction patterns were obtained using a Panalytical X'Pert Pro diffractometer using a Cu K α radiation ($\lambda = 1.5406 \text{ \AA}$) at 40 kV and 40 mA. Spectra data were recorded in the 5–80 2 θ range (step size 0.0167°, time/step = 150 s, total time = 1 h). The nitrogen adsorption isotherms were determined on a Quantachrome autosorb iQ at 77 K. Prior to the analysis, the samples were degassed at 300 °C for 12 h. The specific surface area was calculated using the BET equation. The pore size distribution was calculated using the NLDFT method (the N₂ silica equilibrium transition equation). The vapour sorption was undertaken in the same porosimeter, using water as the solvent, within P/P₀ ranges of 0–0.7. The metal concentration in the zeolite was determined by ICP-MS using an Agilent 7900 ICP-MS (Agilent, Santa Clara, CA, USA) using an HF/HNO₃ matrix solution; approximately 50 mg of the catalyst was immersed in a solution composed of 75 μ L HF (48%) and 250 μ L ultrapure-grade HNO₃ (69%). SEM images were obtained in a Hitachi TM3030 electron microscope using an accelerating voltage of 15 kV and a back-scattering detector. Nuclear Magnetic Resonance (NMR) imaging was carried out in a Bruker Avance III HD 400 MHz NMR spectrometer. ¹¹⁹Sn NMR analyses were carried out at operating frequencies of 149.23 MHz. All of the analysis was run with a 10 kHz spin rate packed in ZrO₂ rotors. The ¹¹⁹Sn DE CPMG MAS NMR experiments were performed with the CPMG echo-train acquisition, as described in Refs. [27,28]. The spectra were measured by applying 100 echoes, using a 2.5 μ s 90° pulse with 180° proton decoupling. The relaxation delay (t₁) used was 135 s with 512 scans. The tin chemical shifts were calibrated using tin (IV) oxide as a reference. DRIFT spectroscopy was performed in a Harrick praying mantis cell. The spectra were recorded on a Bruker Tensor II spectrometer over a range of 4000–600 cm⁻¹ at a resolution of 2 cm⁻¹.

2.5. Kinetic Studies

The retro-aldol fragmentation of D-glucose (Merck Life Science UK Limited, Dorset, UK, $\geq 99\%$) was performed under a continuous flow, in a plug flow stainless steel tubular ($\frac{1}{4}$ " , 4.1 mm ID) reactor [14]. The reactor was connected to an HPLC pump in order to regulate the reactant flow, and to allow operation at an elevated pressure. The catalyst (100 mg) was placed between two plugs of quartz wool and packed in the reactor with a 0.5 μ m frit placed at the reactor outlet. The reactor was then immersed in a thermostatted oil bath at 160 °C. The pressure in the system was controlled using a backpressure regulator, set at the desired pressure (typically 20 bar). Periodic aliquots were taken from the reactor outlet and analysed using an Agilent 1260 Infinity HPLC coupled with a Hi-Plex Ca column and an ELS detector, where sorbitol was used as an external standard. Samples were also measured by GC-FID (Agilent 7820, 25 m CP-Wax 52 CB, Agilent, Santa Clara, CA, USA), for which biphenyl was used as an external standard.

2.6. Activity Definitions

$$\text{Conversion : } X(\%) = \frac{\text{mol}_{\text{Glu}_0} - \text{mol}_{\text{Glu}_t}}{\text{mol}_{\text{Glu}_0}} * 100 \quad (1)$$

$$\text{Yield : } Y(\%) = \frac{\text{mol}_{\text{Product}_t}}{\text{mol}_{\text{Glu}_0}} * 100_{\text{Hexoses or 50ML}} \quad (2)$$

$$\text{Selectivity : } S(\%) = \frac{\text{Product Yield } Y(\%)}{\text{Conversion } X(\%)} * 100 \quad (3)$$

$$\text{Levenspiel deactivation rate : } k_d (\text{h}^{-1}) = \ln \left[\ln \left(\frac{1}{1 - \frac{X(\%)}{100}} \right) \right] \quad (4)$$

$$\text{Turnover frequency : } \text{TOF}_{\text{ML}} (\text{h}^{-1}) = \frac{\text{mol}_{\text{MLt}}}{\text{time (h)} * \text{mol}_{\text{Sn}}} \quad (5)$$

$$\text{Productivity : } P (\text{h}^{-1}) = \frac{m_{\text{ML+MVG}} (\text{g})}{m_{\text{Catalyst}} (\text{g}) * \text{time (h)}} \quad (6)$$

$$\text{Weight hourly space velocity : } \text{WHSV} (\text{h}^{-1}) = \frac{\text{sugar mass feed rate} (\frac{\text{g}}{\text{h}})}{m_{\text{catalyst}} (\text{g})} \quad (7)$$

3. Results and Discussion

3.1. Catalyst Synthesis and Characterisation

A variety of analogous Beta zeolites were first prepared by hydrothermal synthesis according to the established procedures [29]. Within this series, four different metals were chosen as the heteroatom of each material. Specifically, Al-, B-, Ga- and Fe-Beta zeolites were prepared at a target Si/M molar ratio of 200. Additionally, two metal precursors (Al-, B-) were chosen as candidates in order to evaluate the impact of initial heteroatom loading in the parent zeolite; hence, they were also prepared at a target Si/M molar ratio of 100. In order to determine whether all of the parent Beta zeolites were successfully synthesised, XRD patterns were recorded for each sample following the removal of the residual SDA by calcination, and compared with the XRD pattern of a purely siliceous Beta zeolite (i.e., Si-Beta). As can be seen in Figure 1, the XRD patterns of the hydrothermally synthesised Beta zeolites were indistinguishable, and were identical in terms of crystallinity, confirming the successful synthesis of the Beta framework regardless of the choice of starting heteroatom and metal loading.

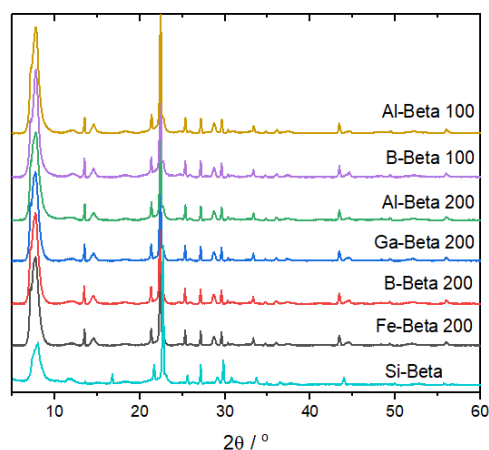


Figure 1. X-Ray Diffraction patterns of Si-Beta and the hydrothermally synthesised M-beta zeolites.

In order to further evaluate the properties of each zeolite, DRIFTS analysis was conducted (Figure 2). All of the synthesised zeolites presented vibrations typical of the Beta framework [30,31]. However, both B-Beta zeolites gave rise to additional vibrations at ca. 910–950 and 3734 cm^{-1} , indicative of Si–O stretching vibrations belonging to uncoupled SiO_4 tetrahedra [32] and internal Si–OH groups present in framework defects, respectively [33]. Further details regarding the presence and absence of vibrations in these materials are reported in Table S1.

In order to determine the impact of the choice of metal on the zeolite morphology, SEM analysis was performed for the Si/M = 200 zeolites (Figure 3). All four samples

were of comparable morphology and size (ca. 10 μm), and possessed the typical trigonal bipyramidal structure of Beta zeolite when synthesised in fluoride media [34].

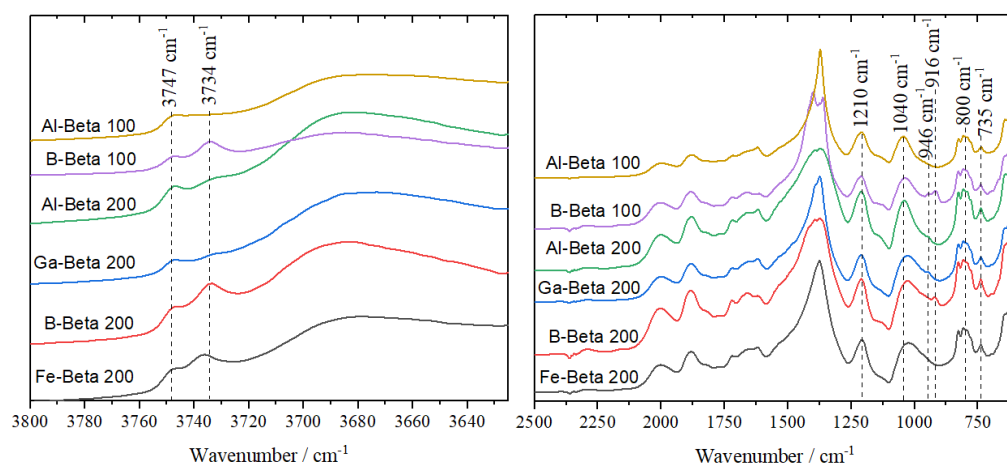


Figure 2. DRIFT spectra of the hydrothermally synthesised M-beta zeolites with Si/M molar ratios of 100 and 200.

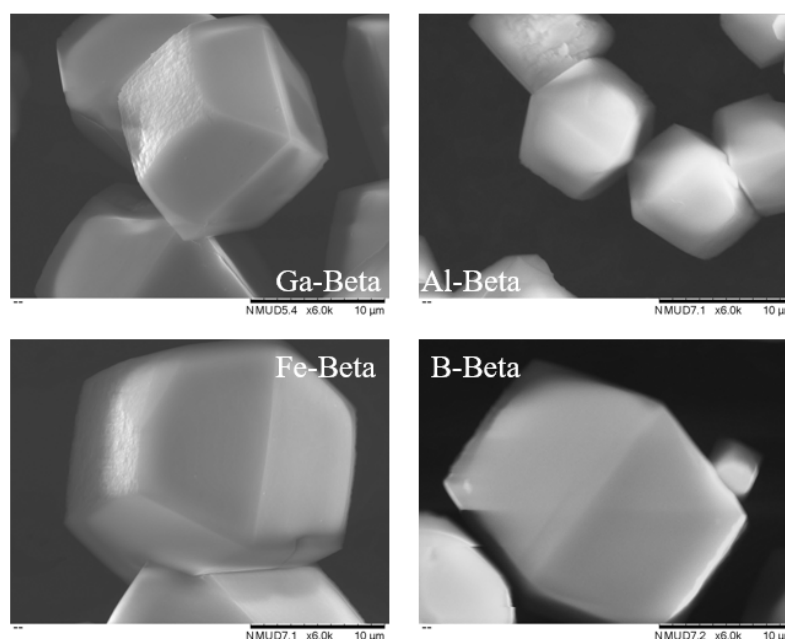


Figure 3. SEM images of hydrothermally synthesised 1Sn-Beta_{M200} zeolites.

The nitrogen physisorption measurements and ICP-MS analyses were also in line with previous studies of Beta zeolites (Table 1). All of the isotherms were typical of microporous Beta zeolites, exhibiting mainly a type I character, but presented some hysteresis in the higher P/P_0 range (Figure S1). The presence of some mesoporosity was confirmed both by Non-linear Density Functional Theory (NLDFT) pore size distribution (PSD) and the t-plot method, as shown in Table 1. All of the samples exhibited comparable Brunauer-Emmett-Teller (BET) surface areas ($S_{\text{BET}} \approx 450\text{--}500 \text{ m}^2 \text{ g}^{-1}$) and micropore volumes ($V_{\text{micro}} \approx 0.20\text{--}0.23 \text{ cm}^3 \text{ g}^{-1}$), irrespective of the original choice of metal (Table 1). Elemental analysis (ICP-MS) showed that all of the parent zeolites contained the anticipated loading heteroatoms, corresponding to an Si/M molar ratio of 200, with the exception of Ga-Beta, which showed a lower Si/M ratio (152), indicating a higher-than-anticipated concentration of Ga in the zeolitic framework. Taken together, XRD, DRIFTS, N_2 physisorption, SEM and ICP-MS confirm that all of the zeolites were successfully synthesised, and possessed

comparable porosity, topology, and composition, making them suitable parent materials for the SSI of Sn.

Table 1. Elemental and textural characteristics of the hydrothermally synthesised M-Beta zeolites, and the subsequent demetallation.

| Catalyst | Si/M ^a | S _{BET} ^b (m ² g ⁻¹) | S _{meso/ext} ^c (m ² g ⁻¹) | V _{total} ^d (cm ³ g ⁻¹) | V _{micro} ^e (cm ³ g ⁻¹) |
|--------------------------|-------------------|--|---|---|---|
| Fe-Beta 200 ^f | 207 | 501 | 59 | 0.32 | 0.23 |
| Ga-Beta 200 ^f | 152 | 504 | 83 | 0.34 | 0.22 |
| Al-Beta 200 ^f | 220 | 463 | 87 | 0.34 | 0.20 |
| B-Beta 200 ^f | 204 | 468 | 13 | 0.32 | 0.22 |
| Al-Beta 100 ^g | 116 | 453 | 46 | 0.34 | 0.21 |
| B-Beta 100 ^g | 107 | 499 | 65 | 0.33 | 0.22 |

^a Experimental Si/M ratio measured by ICP-MS analysis. ^b Surface area values calculated using the BET method.

^c Mesoporous external surface area calculated using the t-plot method. ^d Total pore volume calculated using the t-plot method. ^e Micropore volume calculated from the total pore volume. ^f Theoretical Si/M ratio of 200.

^g Theoretical Si/M molar ratio of 100.

Following their successful synthesis, all of the parental zeolites were demetallated in order to generate the vacant framework sites required for the incorporation of Sn [12]. Although some of the materials can be readily demetallated in mild conditions (particularly B-Beta, which is known to be hydrolytically unstable) [25,35,36], for comparative purposes, all of the parent zeolites described in Table 1 were demetallated by treatment in HNO₃, in accordance with previous studies (13 M HNO₃, 100 °C, 20 h) [13]. ICP-MS confirmed the successful extraction of all of the original heteroatom content in each sample, without major changes to the overall crystallinity of the material (Figure S2).

Following successful demetallation, the SSI of Sn was carried out by grinding the demetallated zeolites with the appropriate quantity of tin (II) acetate to yield a catalyst with a final metal loading 1 wt.% Sn (Si/Sn = 200), prior to heat treatment at 550 °C for a total of 6 h (3 h in N₂ flow followed by 3 h in air flow). The final post-synthetic catalysts were labelled as 1Sn-Beta_{MX}, where M denotes the original metal incorporated into the lattice, i.e., M = B, Al, Fe or Ga, and the X value represents the original Si/M molar ratio of the material. The XRD patterns of the final post-synthetic zeolites showed no changes of the overall crystallinity of the material following demetallation–remetallation (Figure S2). In order to provide further insight as to their respective Sn speciation, ¹¹⁹Sn Magic Angle Spinning Nuclear Magnetic Resonance using the Carr-Purcell-Meiboom-Gill echo train acquisition method (¹¹⁹Sn MAS CPMG NMR) was performed [27,28,37]. Spectra were measured in Direct Excitation (DE) mode, with a relaxation time sufficient to fully relax all of the Sn species in a quantitative manner (t₁ = 135 s) [38]. For comparison, a sample of 1Sn-Beta was also prepared from a commercially available aluminosilicate zeolite Beta (ZeolystTM, Si/M = 19, labelled 1Sn-Beta_{COM19}), which we have extensively characterised and benchmarked over recent years [14,38–40].

The ¹¹⁹Sn DE CPMG MAS NMR spectra of all of the samples presented a number of resonances between –600 and –800 ppm (Figure 4). In particular, all of the samples displayed a resonance characteristic of extra-framework SnO_x species at –600 ppm. Interestingly, out of the hydrothermally synthesised Beta zeolites with a target Si/M ratio of 200, the degallinated analogue exhibited a lower quantity of SnO_x species, which could be a consequence of the initial material having a larger-than-expected quantity of Ga in the lattice of the parental zeolite (Si/M = 154, see Table 1). Moreover, lower quantities of extra-framework Sn sites were also observed for the two zeolites prepared from parental materials with an initial Si/M ratio of 100 (1Sn-Beta_{Al100} and 1Sn-Beta_{B100}, Figures 4 and S3). In addition to the clear trends in terms of the initial Si/M ratio and quantity of extra-framework SnO_x, it is also clear that all of the synthesised samples presented higher quantities of SnO_x than 1Sn-Beta_{COM19}, indicating the incorporation of Sn to be less successful for the parental materials made by fluoride-route hydrothermal synthesis. This could be due to (i) the

even lower Si/M ratio of the commercial material, resulting in a greater number of vacant framework sites following demetallation; (ii) the larger crystallites generated by fluoride media preparation causing the clustering of Sn on the external regions of the material [41]; and/or (iii) differences in the chemical properties of the crystallites (e.g., hydrophobicity), impacting the incorporation mechanism [14,42].

Notably, a variety of other Sn signals resonating in the range of -650 to -737 ppm were also detected in the analysed samples. In general, resonances in this region can all be attributed to Sn atoms isomorphously substituted into the framework in a hydrated state [27,37,43]. However, the precise chemical shift and the relative intensities of these signals varied widely based on the choice of metal and the original Si/M ratio of the material (Al- and B-derived Beta zeolites), even though each material was synthesised at the same loading Sn and by the same preparation method (Figure 4).

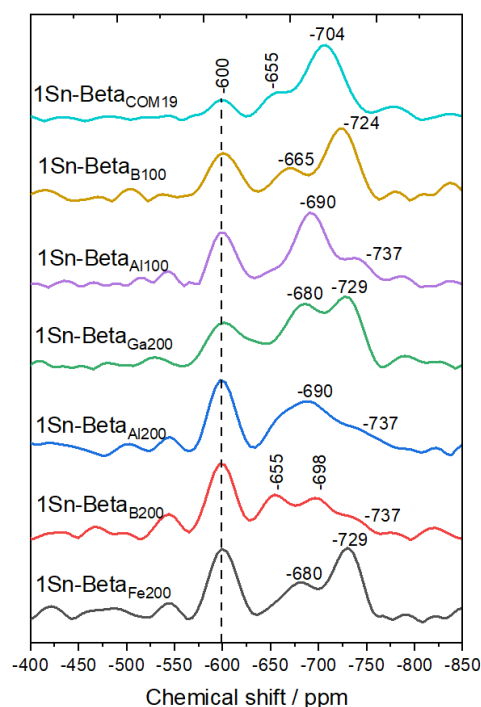


Figure 4. ^{119}Sn DE CPMG MAS NMR spectra of all the post-synthetic $1\text{Sn-Beta}_{\text{MX}}$ zeolites and $1\text{Sn-Beta}_{\text{COM19}}$. Further characterisation details are reported in the experimental section.

Unfortunately, the relationship between the identity of the Sn of the active site(s) within the Beta framework and the chemical shift value observed by ^{119}Sn MAS NMR is still not fully understood, and the scientific community is still divided on this matter [44–47]. However, it is generally appreciated that the different chemical shift values observed in this region arise from the presence of different Sn(IV) species, which could indicate: (i) Sn incorporated in different T-sites of the zeolitic framework; (ii) a different ratio of open or closed sites in the final catalyst; and/or (iii) different quantities of residual fluoride in some materials, which may perturb the Sn species and thus their associated chemical shifts [28,45]. As such, it can generally be concluded from Figure 4 that the identity and concentration of the initial heteroatom in the Beta framework ultimately results in the formation of slightly different active sites in the final Sn-Beta catalyst. However, it can be more specifically concluded that the original Si/M ratio of the parental zeolite is important for the maximisation of the ratio of framework to extra-framework Sn species, and that Sn-Beta catalysts derived from a commercial parental zeolite (i.e., $\text{Sn-Beta}_{\text{COM19}}$) appear to possess a lower quantity of extra-framework SnO_x relative to the counterparts synthesised by the fluoride route.

3.2. Kinetic Evaluation of the Synthesised Catalyst Materials

In order to evaluate the performance of the post-synthetic catalysts, and hence to identify the consequences of the different active site species present in the sample series (Figure 4), the post-synthetic 1Sn-Beta_{MX} series was evaluated for activity regarding the continuous conversion of glucose to α -hydroxy esters (MVG and ML) via retro-aldol fragmentation (Scheme 1). The 1Sn-Beta_{MX} samples were also compared to 1Sn-Beta_{COM19}, which has been used in our previous studies and thus provides context to the experimental trends. The initial experiments were performed in established literature conditions [18,39], using a feed of 1 wt.% glucose in methanol and a reaction temperature of 160 °C. A high Weight Hourly Space Velocity (WHSV = 4.75 h⁻¹) was employed in all of the reactions in order to achieve accurate kinetic data, and the reactions were initially undertaken for a period of two hours of operation in order to gain preliminary insight into the performance of each catalyst. Because many of the intermediate products formed in the retro-aldol fragmentation reaction are challenging to identify by chromatographic methods, the progress of the reaction was determined by measuring the quantity of glucose converted by each catalyst (Equation (1)), and by determining the yields of fructose, mannose, methyl lactate and methyl vinyl glycolate (Equation (2)), because these are known to be the most dominant products formed throughout the cascade reaction (Scheme 1). The overall carbon balance of the effluent solution gathered at the second hour of time on stream was initially used for comparative purposes (Figure 5).

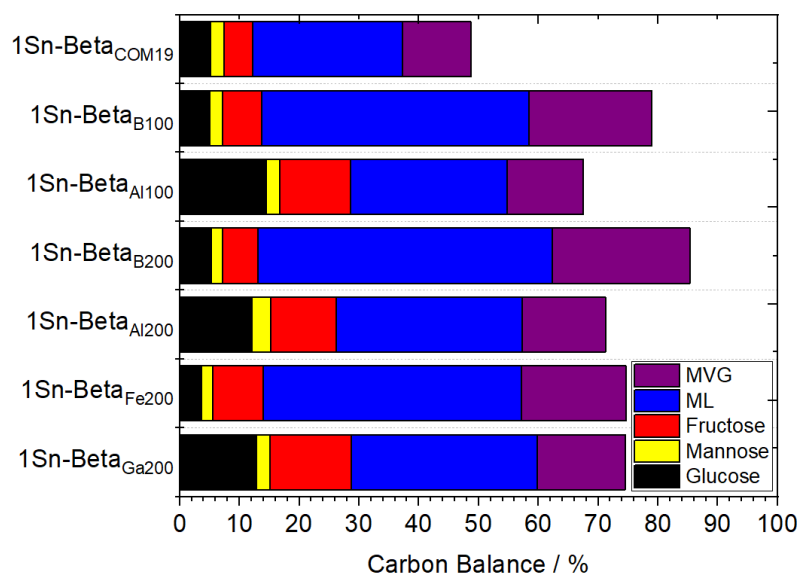


Figure 5. Carbon balance and product distribution achieved following the retro-aldol fragmentation of glucose over post-synthetic 1Sn-Beta_{MX} zeolites. The product distribution was measured at the second hour of time on stream. The reaction conditions were 1 wt.% glucose in methanol, 1 mL min⁻¹ flow rate, 100 mg of the catalyst, and 160 °C. Further details are reported in the experimental section.

Differences in the overall yield of products and reaction selectivity were evident within the 1Sn-Beta_{MX} series. The highest combined yields to retro-aldol products were observed for both B-derived catalyst materials, with 1Sn-Beta_{B200} in particular exhibiting the highest carbon balance due to its enhanced yield of α -hydroxy ester compounds (a combined yield above 70% at 2 h of time on stream). In contrast, the remaining 1Sn-Beta_{MX} catalysts exhibited lower α -hydroxy ester yields of between 35–60%.

However, it is notable that all of the catalysts within the 1Sn-Beta_{MX} series presented much higher initial yields of, and selectivity to, α -hydroxy ester compounds, than those observed for 1Sn-Beta_{COM19}, despite all of the catalysts exhibiting a comparable degree of glucose conversion (approximately 90%). It is thus clear that despite possessing larger quantities of extra-framework SnO_x species (Figure 4), the 1Sn-Beta_{MX} catalyst materi-

als were better-performing catalysts for the retro-aldol fragmentation of glucose than 1Sn-Beta_{COM19} from an activity and selectivity perspective.

In order to acquire a more comprehensive evaluation of the overall catalytic performance and stability of the catalysts, glucose upgrading at 160 °C was performed in a continuous flow for up to 72 h on stream. We note that the operational conditions were established such that the quantity of substrate converted was sub-maximal at the initial hours of the reaction, thereby allowing intrinsic stability to be evaluated, i.e., to avoid an excess catalyst regime [48–50]. Figure 6 presents the time-on-stream data for each catalyst at identical conditions (temperature, flow rate, catalyst mass and, hence, WHSV). As can be seen, all of the catalysts broadly exhibited similar trends during continuous operation, showing an initially rapid rate of deactivation in the first 20 h of reaction, during which the glucose conversion decreased from ca. 95 to 50%, but with activity stabilising thereafter. The loss of activity over the initial reaction period was accompanied by corresponding decreases to the yields of the desired α -hydroxy ester products. The fructose yields increased in this timeframe due to the monosaccharide being an intermediate product in the overall reaction network, and after the first 20 h of time on stream fructose became the main reaction product in all cases.

However, although all of the catalysts showed relatively similar kinetic trends, more detailed analysis of the product distribution revealed that the choice of preparation methodology and starting heteroatom did result in some differences in the activity, selectivity, and stability of the catalyst. For example, Figure 7 presents the α -hydroxy ester (ML and MVG) selectivity as a function of glucose conversion for the various reactions reported in Figure 6. This figure provides a comparison of the combined α -hydroxy ester selectivity for each catalyst at all of the levels of conversion for the analysed materials. Of the catalysts investigated, the ones obtained by means of fluoride synthesis with Al- and B- as starting heteroatoms exhibited better selectivity to α -hydroxy ester compounds, with a selectivity value of approximately 50% obtained at 80% substrate conversion. Interestingly, 1Sn-Beta_{COM19} showed much lower selectivity, displaying only 17% selectivity to the desired esters at the same glucose conversion (80%). This demonstrates how the catalyst synthesised by the commercial precursor is much more prone to catalysing different reaction pathways that are not easily detectable by common chromatographic analysis, resulting in a decreased level of carbon efficiency.

In order to better probe the catalyst stability, the kinetic data presented in Figure 6 were converted to the Levenspiel function (Equation (4)) to calculate the rate of deactivation in each experiment (k_d , Figure 8). Overall, 1Sn-Beta_{COM19} was shown to have the highest rate of deactivation ($k_d = 0.048 \text{ h}^{-1}$), which was approximately 50–60% faster than the rates of deactivation determined for the 1Sn-Beta_{MX} catalyst series. Consequently, the catalyst derived from the commercial zeolite was both less selective (Figure 5) and less stable compared to the catalysts from the 1Sn-Beta_{MX} series. Additionally, a comparison of the α -hydroxy ester productivity of each catalyst ($g_{\text{ML + MVG}} g_{\text{catalyst}}^{-1} \text{ h}^{-1}$) was made (Figure 8). The higher α -hydroxy ester selectivity of 1Sn-Beta_{B200}, coupled with its slightly lower rate of deactivation, resulted in this catalyst presenting a higher productivity per gram of catalyst, which was almost twice as large as that obtained with 1Sn-Beta_{COM19}. Therefore, this material not only offers the possibility of employing a simpler demetallation procedure [23] but also delivers better performance in the process. The ML/MVG molar ratio was determined to be approximately 1.5–2 in all of the cases (Figure S4).

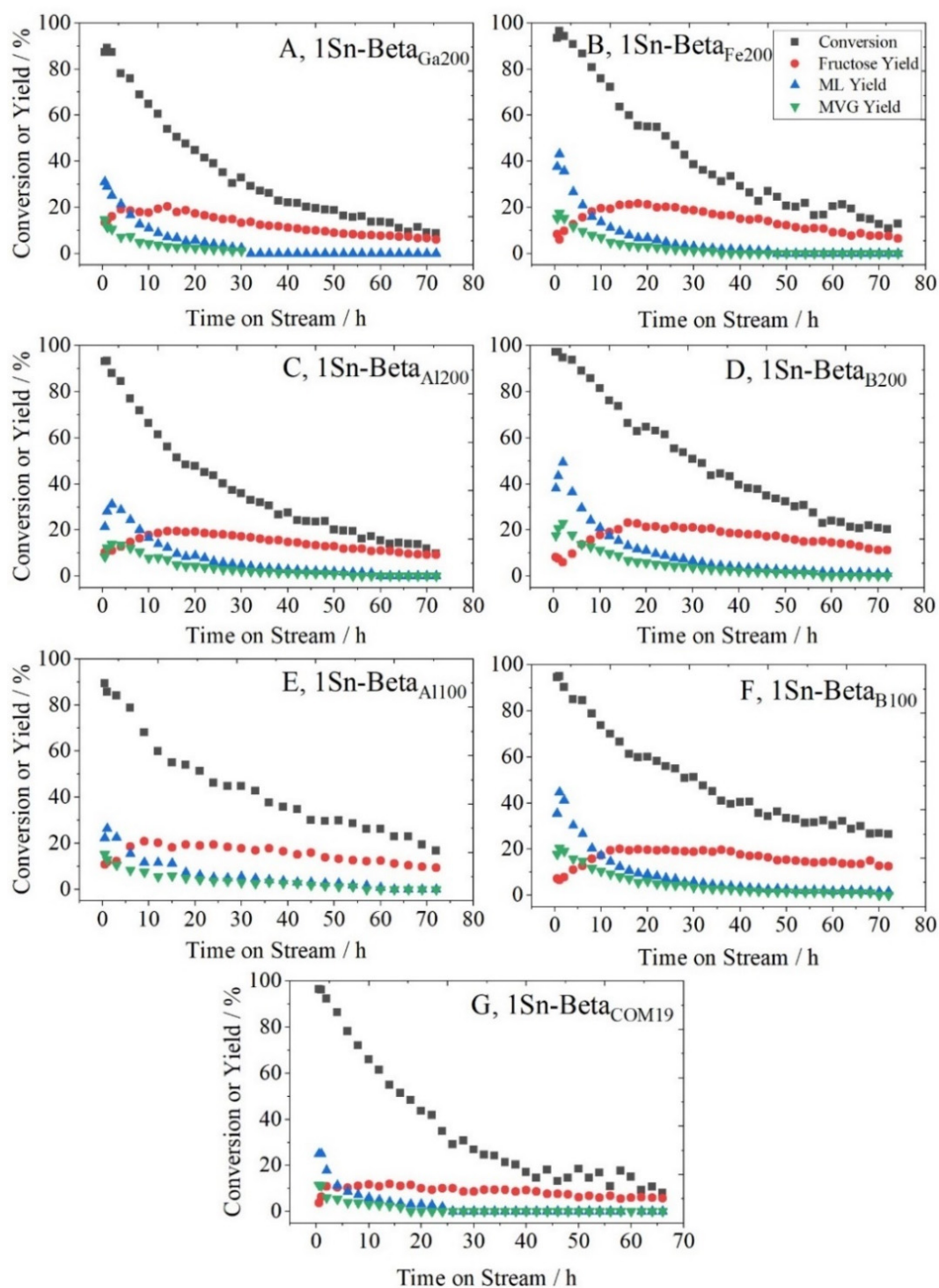


Figure 6. Retro-aldol fragmentation of glucose in a continuous flow over 1Sn-Beta_{MX} and 1Sn-Beta_{COM19} catalysts. (A) 1Sn-Beta_{Ga200}, (B) 1Sn-Beta_{Fe200}, (C) 1Sn-Beta_{Al200}, (D) 1Sn-Beta_{B200}, (E) 1Sn-Beta_{Al100}, (F) 1Sn-Beta_{B100}, and (G) 1Sn-Beta_{COM19}. Reaction conditions: 1 wt.% glucose in methanol, 1 mL min⁻¹ flow rate, 100 mg catalyst, 160 °C. Further details are reported in the experimental section.

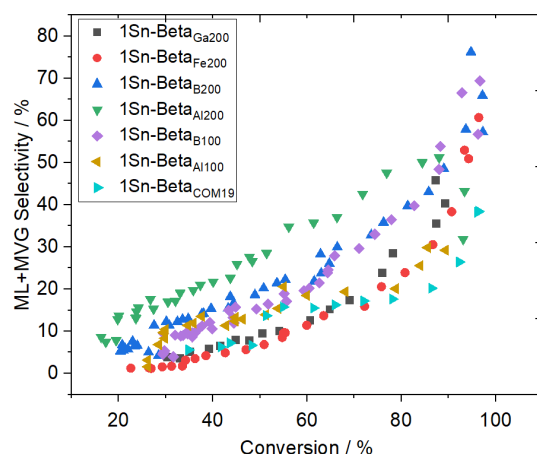


Figure 7. ML + MVG selectivity over glucose conversion for 1Sn-Beta_{MX} and 1Sn-Beta_{COM19}. Reaction conditions: 1 wt.% glucose in methanol, 1 mL min⁻¹ flow rate, 100 mg catalyst, 160 °C. Further details are reported in the experimental section.

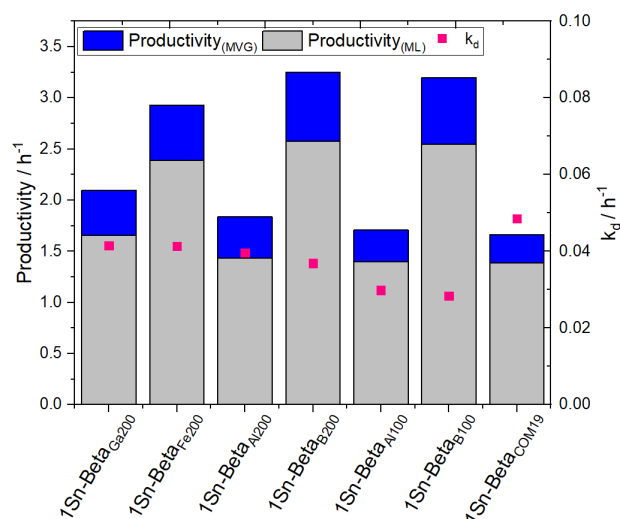


Figure 8. Maximum productivity of ML and MVG per gram of catalyst (bars) and the rate of deactivation (k_d) for each catalyst from the 1Sn-Beta_{MX} series and 1Sn-Beta_{COM19}. The productivity calculations are based on the yield of the respective products at 2 h on stream.

3.3. Effect of Water and Alkali Salts on the Kinetic Performance

The previous section demonstrated how improvement in the activity (productivity), selectivity and stability of post-synthetic Sn-Beta could be achieved by varying the choice and the loading of the heteroatom in the parent M-Beta zeolite. On a balance of these activity indicators [50], the best performance was achieved for Sn-Beta materials prepared from a parental borosilicate Beta zeolite, in particular 1Sn-Beta_{B200}. However, in the conditions described above, the overall yield of retro-aldol products (ML and MVG) obtained from 1Sn-Beta_{B200} decreased from approximately 70–75% at short times on stream (<5 h) to less than 20% after 30 h on stream. Although these yields are comparable to previous reports addressing the catalytic conversion of glucose to α -hydroxy ester compounds, the selectivity and the lifetime of 1Sn-Beta_{B200} towards the production of the desired products (ML and MVG) could be improved.

Towards this objective, previous studies in the literature have shown how slight changes in the reaction conditions can improve the selectivity performance of Sn-Beta for the retro-aldol fragmentation of glucose to α -hydroxy ester compounds, as well as the overall catalyst performance [51–56]. In particular, the addition of alkali salts to the reaction feed has been shown to increase methyl lactate selectivity during the retro-aldol fragmentation

of glucose by a pronounced level [51–54]. In addition, we have shown that an increase in the stability of Sn-Beta catalysts derived from commercial aluminosilicate precursors can be achieved by adding small amounts (1–10% *w/w*) of water to the sugar/MeOH feed, mitigating deactivation under continuous flow reactions [37]. Hence, in order to gauge the potential performance of the 1Sn-Beta_{MX} materials in the presence of these promoters, the retro-aldol fragmentation of glucose over 1Sn-Beta_{B200} was carried out with the addition of KCl (0.335 mol) and water (1:99 H₂O:MeOH *v/v*) to the reaction feed. The concentration of each additive was based on recent studies [39,52]. For these final studies, 1Sn-Beta_{B200} was used as the catalyst, and its performance was compared to 1Sn-Beta_{COM19} following similar perturbation with water and alkali salt. The non-perturbed data (i.e., the activity of both catalysts in the absence of water and alkali salt promoters) is presented in Figure 6.

Figure 9 presents the performance of 1Sn-Beta_{COM19} (A) and 1Sn-Beta_{B200} (B) for glucose conversion at 160 °C in the presence of alkali salt and water promoters. As can be seen, a drastic improvement in performance (glucose conversion and α -hydroxy ester yield) and stability was achieved for both catalysts following the addition of the alkali salt and water to the feed. In particular, the initial yields of ML and MVG increased from 24% and 12% to approximately 60% and 24%, respectively, following the addition of KCl and water to the reaction catalysed by 1Sn-Beta_{COM19}. The consequences of adding water and the alkali salt to the reaction feed were also evaluated for 1Sn-Beta_{B200}. As can be seen, the combined yield of ML and MVG increased from approximately 70% in the absence of the activity promoters to approximately 90% in the presence of water and alkali. The improved performance of 1Sn-Beta_{B200} in the presence of water and KCl was maintained throughout the operational period, with combined yields of ML and MVG > 30% remaining even after 70 h of operation [53].

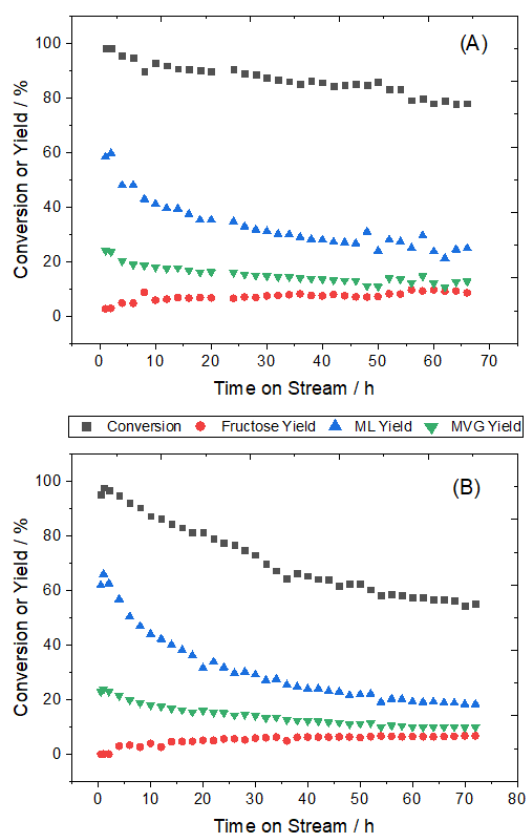


Figure 9. Retro-aldol fragmentation of glucose catalysed by 1Sn-Beta_{COM19} (A) and 1Sn-Beta_{B200} (B) in the presence of alkali salts and water. Reaction conditions: 160 °C, 20 bar, 1% glucose, 99% methanol/water (99:1 *v/v*) solvent with 50 mg KCl (0.335 mmol) per 2 L of solution, and a 1 mL min⁻¹ flow rate per 100 mg catalyst.

In order to elucidate the effect of water and the alkali salt further, the initial carbon balance and the α -hydroxy ester selectivity of both catalysts (1Sn-Beta_{COM19} and 1Sn-Beta_{B200}) were compared in the absence and presence of alkali and water (Figure 10A). In doing so, it is clear that both catalysts showed an increase in selectivity in the presence of water and alkali, which led to α -hydroxy-esters yields above 80% for both materials (Figure 10B), in contrast to yields in the region of 50–60% (for 1Sn-Beta_{COM19}) in the absence of water and KCl. Although both catalysts resulted in higher yields following the addition of water and the alkali salt, Figure 10A showed that the selectivity to α -hydroxy esters at the same rate of conversion was always higher for 1Sn-Beta_{B200} throughout the entire reaction, both in the absence and in the presence of the alkali salt. This indicates that a greater quantity of substrate was converted into undesired products throughout the entire reaction with 1Sn-Beta_{COM19}, leading to a loss of valuable substrate that could otherwise have been recycled post reaction. Furthermore, the addition of alkali salts also significantly decreased the production of the intermediate fructose over 1Sn-Beta_{B200} (Figure S5), whereas 1Sn-Beta_{COM19} yielded a similar selectivity to fructose at the same level of conversion irrespective of whether alkali salts were present. Given the importance of the maximum carbon efficiency during biomass conversion, the improved selectivity of 1Sn-Beta_{B200} throughout the entire reaction coordinate is notable.

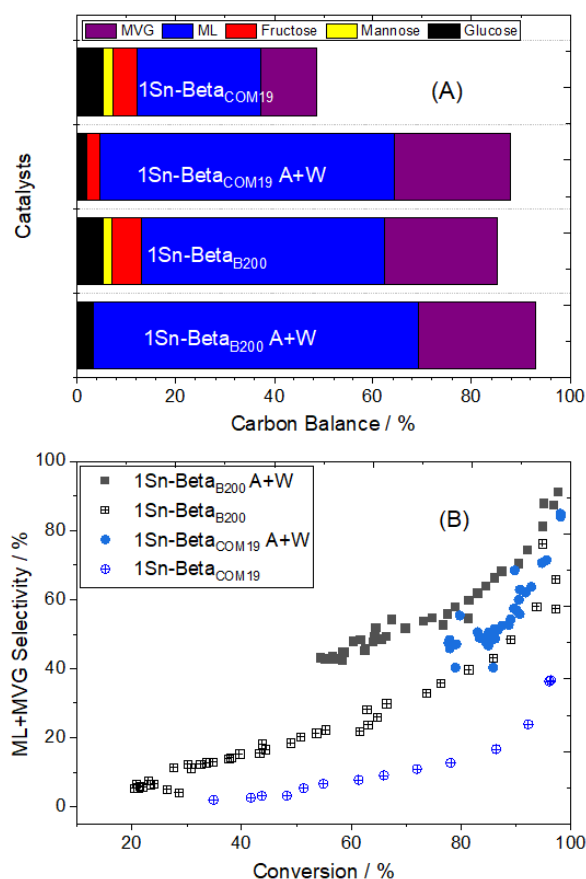


Figure 10. Initial carbon balance (A) and ML + MVG selectivity over glucose conversion (B) using 1Sn-Beta_{B200} and 1Sn-Beta_{COM19} without and with the alkali salt and water (A + W). Reaction conditions: 160 °C, 20 bar, 1 wt.% glucose, 99% methanol/water (99:1 *v/v* %) solvent with 50 mg KCl (0.335 mmol) per 2 L of solution, and a 1 mL min⁻¹ flow rate per 100 mg catalyst.

In contrast, the stability of the material over 72 h of time on stream followed a slightly different trend. In fact, although the addition of water enhanced the stability of both catalysts, the enhancement in stability was greatest for 1Sn-Beta_{COM19}, which experienced only a 20% loss of activity of the reaction period in the presence of water. In contrast,

1Sn-Beta_{B200} experienced a loss of 40% activity over the same 72 h of time on stream. This indicates that the beneficial role of water in the maximisation of stability is somewhat less effective for 1Sn-Beta_{B200} than for 1Sn-Beta_{COM19}, which is likely due to the more hydrophilic characteristics of 1Sn-Beta_{COM19} compared to 1Sn-Beta_{B200}, as evidenced by water sorption studies (Figure S6) [57–59]. The enhanced hydrophilicity of 1Sn-Beta_{COM19} likely favours its interaction with water, and as a result ensures that the promotional effect of water in terms of maximising stability is observed for a longer period.

Based on the results reported in Figures 9 and 10, it is clear that although the addition of water and alkali was beneficial for both 1Sn-Beta_{COM19} and 1Sn-Beta_{B200}, the better performance of 1Sn-Beta_{B200} makes it much less reliant on the use of activity promoters than the commercially-derived analogue. Moreover, the improved selectivity of 1Sn-Beta_{B200} in all of the tested conditions is evident. Thus, it is clear that despite possessing a less homogeneous distribution of active Sn sites, and hence likely containing a lower quantity of active Sn sites per gram of catalyst, the catalyst derived from B-containing Beta zeolite is the most favourable catalyst for the retro-aldol fragmentation of glucose amongst the materials studied in this report.

4. Conclusions

This study focuses on how the choice of starting zeolite material impacts the preparation and performance of post-synthetic Sn-Beta catalysts prepared by solid-state incorporation for the retro-aldol fragmentation of glucose. In particular, four different metal-incorporated Beta zeolites (M-Beta, M = Ga-, Fe-, B-, Al-) were explored as parent materials for the top-down synthesis of Sn-Beta via demetallation–remetallation, and their ultimate performances were explored for the retro-aldol fragmentation of glucose to the α -hydroxy ester compounds methyl lactate and methyl vinyl glycolate. ¹¹⁹Sn MAS DE CPMG NMR, alongside XRD, IR, DRIFTS, ICP-MS and porosimetry analysis, demonstrated the successful synthesis of Sn-Beta in all of the cases, albeit with a wide array of different isomorphously-substituted Sn species being present in each sample.

The kinetic performance of each catalyst was evaluated in a continuous flow reactor, and revealed that all of the synthesised materials were active for this reaction, and hence, that different metal precursors can be employed as starting materials for the synthesis of Sn-Beta by SSI. The catalyst synthesised from the B-Beta starting material was shown to exhibit the best performance in terms of productivity and selectivity to the desired α -hydroxy-ester compounds.

Based on these findings, we can conclude that B-derived zeolites are a feasible alternative to Al-containing zeolites for SSI. This finding may be advantageous in the long term, because the hydrolytically unstable nature of borosilicate zeolites has been shown to result in their easier demetallation compared to their aluminosilicate analogues, potentially avoiding the use of highly acidic reaction solutions to remove the original heteroatom from the zeolite lattice during demetallation.

Along with identifying that B-containing materials exhibit a higher potential to act as parental zeolites for solid-state incorporation, this study also reveals broader guidelines for the successful synthesis of Sn-Beta catalysts. Namely, although ¹¹⁹Sn MAS DE CPMG NMR suggested that the 1Sn-Beta_{MX} series possessed a less favourable distribution of active sites than the catalyst derived from commercial Al-Beta (1Sn-Beta_{COM19}), this series nevertheless presented higher levels of activity and stability compared to the commercially-derived counterpart. Although this trend was somewhat reversed when activity promoters were added to the solution, this suggests that the different lattice properties achieved through the fluoride medium preparation (i.e., increased hydrophobicity, decreased defect site density, larger crystallite sizes) are more determining in terms of the achievement of high performance without resorting to activity promoters.

Supplementary Materials: The following supporting information can be downloaded at <https://www.mdpi.com/article/10.3390/reactions3020020/s1>. Figure S1: Nitrogen sorption isotherm and pore size distribution using the DFT model (inset) of parent M-Beta zeolites. Figure S2: X-Ray Diffraction patterns of calcined B-Beta parent material, demetallated Beta derived from B-Beta, and Sn-Beta achieved by SSI of demetallated B-Beta. Figure S3: ^{119}Sn De CPMG MAS NMR spectra of $1\text{Sn-Beta}_{\text{M}100}$ and $1\text{Sn-Beta}_{\text{M}200}$ where $\text{M}=\text{B}$ (left) and $\text{M}=\text{Al}$ (right). Figure S4: ML/MVG ratio over glucose conversion for the $1\text{Sn-Beta}_{\text{M}x}$ series and $1\text{SnBeta}_{\text{COM}19}$. Figure S5: Comparison of the fructose selectivity over glucose conversion of the original ML fragmentation and ML fragmentation with alkali salts and water (A + W). Figure S6: Vapour sorption data of various 1Sn-Beta catalysts, including (red/circles) $1\text{Sn-Beta}_{\text{COM}19}$, (blue/triangles) $1\text{Sn-Beta}_{\text{B}200}$ and (squares/black) hydrothermally synthesised $1\text{Sn-Beta}_{\text{HDT}}$, which is provided for reference purposes only. Table S1: Principal modes and assignments of hydrothermal M-Beta zeolites.

Author Contributions: Conceptualization, C.H.; Data curation, R.N. and L.B.; Formal analysis, R.N., L.B., G.T. and C.H.; Funding acquisition, R.N. and C.H.; Methodology, L.B. and C.H.; Supervision, C.H.; Visualization, R.N.; Writing—original draft, R.N., L.B. and G.T.; Writing—review & editing, G.T. and C.H. All authors have read and agreed to the published version of the manuscript.

Funding: C.H. gratefully appreciates the support of The Royal Society, for the provision of a University Research Fellowship (UF140207, URF/R/201003) and enhanced research grant funding (RGF/EA/180314). C.H. and R.N. appreciate the support of Consejo Nacional de Ciencia y Tecnología (Fellowship 472256) for PhD studentship funding.

Institutional Review Board Statement: Not applicable.

Informed Consent Statement: Not applicable.

Data Availability Statement: Not applicable.

Conflicts of Interest: The authors declare no conflict of interest.

References

1. Pachamuthu, M.P.; Shanthi, K.; Luque, R.; Ramanathan, A. SnTUD-1: A solid acid catalyst for three component coupling reactions at room temperature. *Green Chem.* **2013**, *15*, 2158–2166. [CrossRef]
2. Corma, A.; Domine, M.E.; Nemeth, L.; Valencia, S. Al-Free Sn-Beta Zeolite as a Catalyst for the Selective Reduction of Carbonyl Compounds (Meerwein-Ponndorf-Verley Reaction). *J. Am. Chem. Soc.* **2002**, *124*, 3194–3195. [CrossRef] [PubMed]
3. Takahara, I.; Saito, M.; Inaba, M.; Murata, K. Dehydration of Ethanol into Ethylene over Solid Acid Catalysts. *Catal. Lett.* **2005**, *105*, 249–252. [CrossRef]
4. Esteban, J.; Yustos, P.; Ladero, M. Catalytic Processes from Biomass-Derived Hexoses and Pentoses: A Recent Literature Overview. *Catalysts* **2018**, *8*, 637. [CrossRef]
5. Li, Y.-P.; Head-Gordon, M.; Bell, A.T. Analysis of the Reaction Mechanism and Catalytic Activity of Metal-Substituted Beta Zeolite for the Isomerization of Glucose to Fructose. *ACS Catal.* **2014**, *4*, 1537–1545. [CrossRef]
6. Moliner, M.; Roman-Leshkov, Y.; Davis, M.E. Tin-containing zeolites are highly active catalysts for the isomerization of glucose in water. *Proc. Natl. Acad. Sci. USA* **2010**, *107*, 6164–6168. [CrossRef]
7. Zhang, J.; Wang, L.; Wang, G.; Chen, F.; Zhu, J.; Wang, C.; Bian, C.; Pan, S.; Xiao, F.-S. Hierarchical Sn-Beta Zeolite Catalyst for the Conversion of Sugars to Alkyl Lactates. *ACS Sustain. Chem. Eng.* **2017**, *5*, 3123–3131. [CrossRef]
8. Yang, X.; Liu, Y.; Li, X.; Ren, J.; Zhou, L.; Lu, T.; Su, Y. Synthesis of Sn-Containing Nanosized Beta Zeolite as Efficient Catalyst for Transformation of Glucose to Methyl Lactate. *ACS Sustain. Chem. Eng.* **2018**, *6*, 8256–8265. [CrossRef]
9. De Clercq, R.; Dusselier, M.; Christiaens, C.; Dijkmans, J.; Iacobescu, R.I.; Pontikes, Y.; Sels, B.F. Confinement Effects in Lewis Acid-Catalyzed Sugar Conversion: Steering Toward Functional Polyester Building Blocks. *ACS Catal.* **2015**, *5*, 5803–5811. [CrossRef]
10. Pérez-Ramírez, J.; Groen, J.C.; Brückner, A.; Kumar, M.S.; Bentrup, U.; Debbagh, M.N.; Villaescusa, L.A. Evolution of isomorphously substituted iron zeolites during activation: Comparison of Fe-beta and Fe-ZSM-5. *J. Catal.* **2005**, *232*, 318–334. [CrossRef]
11. Müller, M.; Harvey, G.; Prins, R. Comparison of the dealumination of zeolites beta, mordenite, ZSM-5 and ferrierite by thermal treatment, leaching with oxalic acid and treatment with SiCl_4 by ^1H , ^{29}Si and ^{27}Al MAS NMR. *Micropor. Mesopor. Mater.* **2000**, *34*, 135–147. [CrossRef]
12. Wolf, P.; Hammond, C.; Conrad, S.; Hermans, I. Post-synthetic preparation of Sn-, Ti- and Zr-beta: A facile route to water tolerant, highly active Lewis acidic zeolites. *Dalton Trans.* **2014**, *43*, 4514–4519. [CrossRef] [PubMed]
13. Hammond, C.; Conrad, S.; Hermans, I. Simple and Scalable Preparation of Highly Active Lewis Acidic Sn- β . *Angew. Chem. Int. Ed.* **2012**, *51*, 11736–11739. [CrossRef] [PubMed]

14. Botti, L.; Navar, R.; Tolborg, S.; Martinez-Espin, J.S.; Padovan, D.; Taarning, E.; Hammond, C. Influence of Composition and Preparation Method on the Continuous Performance of Sn-Beta for Glucose-Fructose Isomerisation. *Top. Catal.* **2018**, *62*, 1178–1191. [[CrossRef](#)]
15. Losch, P.; Hoff, T.C.; Kolb, J.F.; Bernardon, C.; Tessonnier, J.-P.; Louis, B. Mesoporous ZSM-5 Zeolites in Acid Catalysis: Top-Down vs. Bottom-Up Approach. *Catalysts* **2017**, *7*, 225. [[CrossRef](#)]
16. Tang, B.; Dai, W.; Sun, X.; Wu, G.; Guan, N.; Hunger, M.; Li, L. Mesoporous Zr-Beta zeolites prepared by a post-synthetic strategy as a robust Lewis acid catalyst for the ring-opening aminolysis of epoxides. *Green Chem.* **2015**, *17*, 1744–1755. [[CrossRef](#)]
17. Tang, B.; Dai, W.; Sun, X.; Guan, N.; Li, L.; Hunger, M. A procedure for the preparation of Ti-Beta zeolites for catalytic epoxidation with hydrogen peroxide. *Green Chem.* **2014**, *16*, 2281–2291. [[CrossRef](#)]
18. Van der Graaff, W.N.P.; Tempelman, C.H.L.; Hendriks, F.C.; Ruiz-Martinez, J.; Bals, S.; Weckhuysen, B.M.; Pidko, E.A.; Hensen, E.J.M. Deactivation of Sn-Beta during carbohydrate conversion. *Appl. Catal. A Gen.* **2018**, *564*, 113–122. [[CrossRef](#)]
19. Kucherov, A.V.; Slinkin, A.A. Solid-state reaction as a way to transition metal cation introduction into high-silica zeolites. *J. Mol. Catal.* **1994**, *90*, 323–354. [[CrossRef](#)]
20. Van Bokhoven, J.A.; Koningsberger, D.C.; Kunkeler, P.; Van Bekkum, H.; Kentgens, A.P.M. Stepwise Dealumination of Zeolite Beta at Specific T-Sites Observed with ^{27}Al MAS and ^{27}Al MQ MAS NMR. *J. Am. Chem. Soc.* **2000**, *122*, 12842–12847. [[CrossRef](#)]
21. Escola, J.M.; Serrano, D.P.; Sanz, R.; Garcia, R.A.; Peral, A.; Moreno, I.; Linares, M. Synthesis of hierarchical Beta zeolite with uniform mesopores: Effect on its catalytic activity for veratrole acylation. *Catalysts* **2018**, *304*, 89–96. [[CrossRef](#)]
22. Zhu, Z.; Xu, H.; Jiang, J.; Guan, Y.; Wu, P. Sn-Beta zeolite derived from a precursor synthesized via an organotemplate-free route as efficient Lewis acid catalyst. *Appl. Catal. A Gen.* **2018**, *556*, 52–63. [[CrossRef](#)]
23. Koller, H.; Senapati, S.; Ren, J.; Uesbeck, T.; Siozios, V.; Hunger, M.; Lobo, R.F. Post-Synthesis Conversion of Borosilicate Zeolite Beta to an Aluminosilicate with Isolated Acid Sites: A Quantitative Distance Analysis by Solid-State NMR. *J. Phys. Chem. C* **2016**, *120*, 9811–9820. [[CrossRef](#)]
24. Ranoux, A.; Djanashvili, K.; Arends, I.W.C.E.; Hanefeld, U. B-TUD-1: A versatile mesoporous catalyst. *RSC Adv.* **2013**, *3*, 21524–21534. [[CrossRef](#)]
25. De Ruiter, R.; Kentgens, A.P.M.; Grootendorst, J.; Jansen, J.C.; van Bekkum, H. Calcination and deboronation of [B]-MFI single crystals. *Zeolites* **1993**, *13*, 128–138. [[CrossRef](#)]
26. Hammond, C.; Padovan, D.; Al-Nayili, A.; Wells, P.P.; Gibson, E.K.; Dimitratos, N. Identification of Active and Spectator Sn Sites in Sn- β Following Solid-State Stannation, and Consequences for Lewis Acid Catalysis. *ChemCatChem* **2015**, *7*, 3322–3331. [[CrossRef](#)]
27. Kolyagin, Y.G.; Yakimov, A.V.; Tolborg, S.; Vennestrøm, P.N.R.; Ivanova, I.I. Application of ^{119}Sn CPMG MAS NMR for Fast Characterization of Sn Sites in Zeolites with Natural ^{119}Sn Isotope Abundance. *J. Phys. Chem. Lett.* **2016**, *7*, 1249–1253. [[CrossRef](#)]
28. Yakimov, A.V.; Kolyagin, Y.G.; Tolborg, S.; Vennestrøm, P.N.R.; Ivanova, I.I. ^{119}Sn MAS NMR Study of the Interaction of Probe Molecules with Sn-BEA: The Origin of Penta- and Hexacoordinated Tin Formation. *J. Phys. Chem. C* **2016**, *120*, 28083–28092. [[CrossRef](#)]
29. Tolborg, S.; Katerinopoulou, A.; Falcone, D.D.; Sádaba, I.; Osmundsen, C.M.; Davis, R.J.; Taarning, E.; Fristrup, P.; Holm, M.S. Incorporation of tin affects crystallization, morphology, and crystal composition of Sn-Beta. *J. Mater. Chem. A* **2014**, *2*, 20252–20262. [[CrossRef](#)]
30. Flanigen, E.M.; Khatami, H.; Szymanski, H.A. Molecular Sieve Zeolites-I. In *Advances in Chemistry*; American Chemical Society: Washington, DC, USA, 1974; pp. 16–201.
31. Tomlinson, S.R.; McGown, T.; Schlup, J.R.; Anthony, J.L. Infrared Spectroscopic Characterization of CIT-6 and a Family of *BEA Zeolites. *Int. J. Spectrosc.* **2013**, *2013*, 961404. [[CrossRef](#)]
32. Chalupka, K.; Sadek, R.; Valentin, L.; Millot, Y.; Calers, C.; Nowosielska, M.; Rynkowski, J.; Dzwigaj, S. Dealuminated Beta Zeolite Modified by Alkaline Earth Metals. *J. Chem.* **2018**, *2018*, 7071524. [[CrossRef](#)]
33. Kiricsi, I.; Flego, C.; Pazzuconi, G.; Parker, W.O.; Millini, R.; Perego, C.; Bellussi, G. Progress toward Understanding Zeolite β Acidity: An IR and ^{27}Al NMR Spectroscopic Study. *J. Phys. Chem.* **1994**, *98*, 4627–4634. [[CrossRef](#)]
34. Xia, Q.H.; Song, J.; Kawi, S.; Li, L.L. Characterization and morphological control of β zeolite synthesized in a fluoride medium. *Stud. Surf. Sci. Catal.* **2004**, *154*, 195–202. [[CrossRef](#)]
35. Tong, H.T.T.; Koller, H. Control of Al for B framework substitution in zeolite Beta by counterions. *Micropor. Mesopor. Mater.* **2012**, *148*, 80–87. [[CrossRef](#)]
36. Hamoudi, S.; Larachi, F.; Sayari, A. Synthesis and Characterization of Titanium-Substituted Large Pore SSZ-42 Zeolite. *Catal. Lett.* **2001**, *77*, 227–231. [[CrossRef](#)]
37. Padovan, D.; Botti, L.; Hammond, C. Active Site Hydration Governs the Stability of Sn-Beta during Continuous Glucose Conversion. *ACS Catal.* **2018**, *8*, 7131–7140. [[CrossRef](#)]
38. Botti, L.; Padovan, D.; Navar, R.; Tolborg, S.; Martinez-Espin, J.S.; Hammond, C. Thermal Regeneration of Sn-Containing Silicates and Consequences for Biomass Upgrading: From Regeneration to Preactivation. *ACS Catal.* **2020**, *10*, 11545–11555. [[CrossRef](#)]
39. Padovan, D.; Tolborg, S.; Botti, L.; Taarning, E.; Sádaba, I.; Hammond, C. Overcoming catalyst deactivation during the continuous conversion of sugars to chemicals: Maximising the performance of Sn-Beta with a little drop of water. *React. Chem. Eng.* **2018**, *3*, 155–163. [[CrossRef](#)]

40. Padovan, D.; Parsons, C.; Simplicio Grasina, M.; Hammond, C. Intensification and deactivation of Sn-beta investigated in the continuous regime. *Green Chem.* **2016**, *18*, 5041–5049. [[CrossRef](#)]
41. Kalvachev, Y.; Jaber, M.; Mavrodinova, V.; Dimitrov, L.; Nihtianova, D.; Valtchev, V. Seeds-induced fluoride media synthesis of nanosized zeolite Beta crystals. *Micropor. Mesopor. Mater.* **2013**, *177*, 127–134. [[CrossRef](#)]
42. Botti, L.; Navar, R.; Tolborg, S.; Martinez-Espin, J.S.; Hammond, C. High-Productivity Continuous Conversion of Glucose to α -Hydroxy Esters over Postsynthetic and Hydrothermal Sn-Beta Catalysts. *ACS Sustain. Chem. Eng.* **2022**, *10*, 4391–4403. [[CrossRef](#)] [[PubMed](#)]
43. Bermejo-Deval, R.; Gounder, R.; Davis, M.E. Framework and Extraframework Tin Sites in Zeolite Beta React Glucose Differently. *ACS Catal.* **2012**, *2*, 2705–2713. [[CrossRef](#)]
44. Wolf, P.; Valla, M.; Núñez-Zarur, F.; Comas-Vives, A.; Rossini, A.J.; Firth, C.; Kallas, H.; Lesage, A.; Emsley, L.; Copéret, C.; et al. Correlating Synthetic Methods, Morphology, Atomic-Level Structure, and Catalytic Activity of Sn- β Catalysts. *ACS Catal.* **2016**, *6*, 4047–4063. [[CrossRef](#)]
45. Hwang, S.J.; Gounder, R.; Bhawe, Y.; Orazov, M.; Bermejo-Deval, R.; Davis, M.E. Solid State NMR Characterization of Sn-Beta Zeolites that Catalyze Glucose Isomerization and Epimerization. *Top. Catal.* **2015**, *58*, 435–440. [[CrossRef](#)]
46. Kolyagin, Y.G.; Yakimov, A.V.; Tolborg, S.; Vennestrøm, P.N.R.; Ivanova, I.I. Direct Observation of Tin in Different T-Sites of Sn-BEA by One- and Two-Dimensional ^{119}Sn MAS NMR Spectroscopy. *J. Phys. Chem. Lett.* **2018**, *9*, 3738–3743. [[CrossRef](#)] [[PubMed](#)]
47. Corma, A.; Nemeth, L.T.; Renz, M.; Valencia, S. Sn-zeolite beta as a heterogeneous chemoselective catalyst for Baeyer–Villiger oxidations. *Nature* **2001**, *412*, 423–425. [[CrossRef](#)] [[PubMed](#)]
48. Zhang, Y.; Luo, H.; Zhao, X.; Zhu, L.; Miao, G.; Wang, H.; Li, S.; Kong, L. Continuous Conversion of Glucose into Methyl Lactate over the Sn-Beta Zeolite: Catalytic Performance and Activity Insight. *Ind. Eng. Chem. Res.* **2020**, *59*, 17365–17372. [[CrossRef](#)]
49. Scott, S.L. A Matter of Life(time) and Death. *ACS Catal.* **2018**, *8*, 8597–8599. [[CrossRef](#)]
50. Hammond, C. Intensification studies of heterogeneous catalysts: Probing and overcoming catalyst deactivation during liquid phase operation. *Green Chem.* **2017**, *19*, 2711–2728. [[CrossRef](#)]
51. Tolborg, S.; Sádaba, I.; Osmundsen, C.M.; Fristrup, P.; Holm, M.S.; Taarning, E. Tin-containing Silicates: Alkali Salts Improve Methyl Lactate Yield from Sugars. *ChemSusChem*. **2015**, *8*, 613–617. [[CrossRef](#)]
52. Elliot, S.G.; Tolborg, S.; Madsen, R.; Taarning, E.; Meier, S. Effects of Alkali and Counter Ions in Sn-Beta Catalyzed Carbohydrate Conversion. *ChemSusChem* **2018**, *11*, 1198–1203. [[CrossRef](#)] [[PubMed](#)]
53. Elliot, S.G.; Tosi, I.; Meier, S.; Martinez-Espin, J.S.; Tolborg, S.; Taarning, E. Stoichiometric active site modification observed by alkali ion titrations of Sn-Beta. *Catal. Sci. Technol.* **2019**, *9*, 4339–4346. [[CrossRef](#)]
54. Yang, Q.; Lan, W.; Runge, T. Salt-Promoted Glucose Aqueous Isomerization Catalyzed by Heterogeneous Organic Base. *ACS Sustain. Chem. Eng.* **2016**, *4*, 4850–4858. [[CrossRef](#)]
55. Furushiro, Y.; Kobayashi, T. Reaction Behavior of Glucose and Fructose in Subcritical Water in the Presence of Various Salts. *J. Appl. Glycosci.* **2020**, *67*, 11–15. [[CrossRef](#)]
56. Yoo, C.G.; Li, N.; Swannell, M.; Pan, X. Isomerization of glucose to fructose catalyzed by lithium bromide in water. *Green Chem.* **2017**, *19*, 4402–4411. [[CrossRef](#)]
57. Vega-Vila, C.; Harris, J.W.; Gounder, R. Controlled insertion of tin atoms into zeolite framework vacancies and consequences for glucose isomerization catalysis. *J. Catal.* **2016**, *344*, 108–120. [[CrossRef](#)]
58. Humplik, T.; Raj, R.; Maroo, S.C.; Laoui, T.; Wang, E.N. Effect of Hydrophilic Defects on Water Transport in MFI Zeolites. *Langmuir* **2014**, *30*, 6446–6453. [[CrossRef](#)]
59. Zhu, Z.; Xu, H.; Jiang, J.; Wu, H.; Wu, P. Hydrophobic Nanosized All-Silica Beta Zeolite: Efficient Synthesis and Adsorption Application. *ACS Appl. Mater. Interfaces* **2017**, *9*, 27273–27283. [[CrossRef](#)]